Photothermal-Plasmonic Catalysis at Liquid-Liquid Interfaces: Enhancing and Steering Biphasic Reactions with Light

Zhi Zhong Ang [a], Veronica Pereira [a], Li Shiuan Ng [a], Carice Chong [a], Haitao Li [b], Hongjian Yu [b], and Hiang Kwee Lee [a] [c] [d]*

[a] Division of Chemistry and Biological Chemistry, School of Chemistry, Chemical Engineering and Biotechnology, Nanyang Technological University, 21 Nanyang Link, Singapore 637371 (Singapore)

[b] School of Chemistry and Chemical Engineering, Yangzhou University, Yangzhou, 25002 (P. R. China)

[c] Institute of Materials Research and Engineering, The Agency for Science, Technology and Research (A*STAR), 2 Fusionopolis Way, #08-03, Innovis, Singapore 138634 (Singapore)

[d] Centre for Hydrogen Innovations, National University of Singapore, E8, 1 Engineering Drive 3, Singapore 117580 (Singapore)

*Correspondence to: hiangkwee@ntu.edu.sg

Keywords: biphasic catalysis • liquid−liquid interface • nanoparticle • plasmonic • photothermal

Abstract

Phase-boundary catalysis strategically positions heterogeneous nanocatalysts at immiscible liquid-liquid interfaces to facilitate reactions between reactants with polarity disparity. However, current designs are limited by low catalytic activity, poor interfacial stability, difficulty in heating without disrupting the catalyst layer, and hydrolytic degradation of reactive intermediates in water. Herein, we achieve efficient phase-boundary catalysis by employing nanoporous gold bowls (NPGBs) with strong plasmonic and photothermal properties to control and enhance interfacial reactions using light. Our strategy integrates two key concepts: (1) NPGBs act as photothermal nanoheaters, localizing heat at the liquid-liquid interface to drive reactions while preserving the stability of the interfacial layer; (2) they also function as plasmonic catalysts, generating hot carriers to accelerate reaction and direct chemical pathways. Using the reduction of 4-nitroaniline by $NaBH_4$ as a model, this approach achieves ~36-fold increase in reactant consumption and reaching up to 92% conversion to para-phenylenediamine under optimal conditions. Mechanistic investigations show that 90% of the catalytic enhancement arises from plasmonic and photothermal effects, with hot electrons enriching active surface hydride species by suppressing undesired hydrolysis to H_2. This work underscores the immense potential of photothermal-plasmonic catalysis to advance and manipulate multiphasic reactions using light for diverse chemical, environmental, and energy applications.

Introduction

Biphasic liquid-liquid reactions offer an effective platform for molecular transformations by enabling chemical reactions at the interface between reactants dissolved in two immiscible solvents. This interfacial approach brings together reactants with extreme polarity disparities, allowing access to abundant and environmentally benign reagents and facilitating reactions that are otherwise challenging or inefficient in traditional single-phase systems.[1-5] Among biphasic methods, phase-boundary catalysis stands out as a promising approach, employing amphiphilic heterogeneous catalysts (e.g., zeolites and titania particles) precisely positioned at the liquid-liquid interface.[6-10] Unlike conventional phase-transfer catalysis which relies on a homogeneous catalyst that must shuttle between phases,[4, 11-15] the formation of the liquid-catalyst-liquid interface in phase-boundary catalysis maximizes interactions between the catalyst and reactants from each phase for enhanced interfacial organic reactions. Additionally, the fixed positioning of the solid catalyst at the interface simplifies recovery and supports reusability, avoiding the complex post-reaction separations often necessary for phase-transfer catalysts. These benefits make phase-boundary catalysis highly effective for diverse organic transformations, such as hydroformylation and alkene epoxidation, with important industrial importance.

Despite its potential for greener chemistry, current phase-boundary catalysis faces critical challenges in achieving efficient catalytic performance, often necessitating high reactant concentrations to effectively drive reactions.[16, 17] These limitations arise from several intrinsic constraints within phase-boundary catalytic systems. First, the interfacial catalyst layer generally has lower catalytic activity compared to homogeneous phase-transfer catalysts, primarily due to fewer active sites on heterogeneous catalysts. Second, the need to maintain a stable catalyst layer at the interface restricts biphasic reactions to static and ambient conditions, making it difficult to

use mechanical agitation (e.g., stirring) to ensure efficient mass transfer. While emulsification can increase interfacial mass transfer, it adds complexity to post-reaction separation as products and catalysts must be recovered from both continuous and dispersed phases.[6, 7, 18] Third, bulk heating to accelerate reaction kinetics presents further complications, where convection currents generated in each liquid phase can destabilize the interfacial catalyst layer and reduce reaction efficiency.[19] Finally, a major drawback common in biphasic reactions is the susceptibility of valuable reaction intermediates to hydrolysis or degradation in water, a common solvent in biphasic systems.[20, 21] For instance, reactive hydrogen (H) adatoms essential for reduction reactions may be prematurely quenched by water, generating H_2 gas and diminishing the intended reaction's efficiency.[22-25] These challenges underscore the need for new approaches to improve catalytic activity and process selectivity in phase-boundary catalysis.

Herein, we achieve efficient phase-boundary catalysis by incorporating nanoporous gold bowl (NPGB) catalysts with strong plasmonic and photothermal properties to manipulate interfacial reactions at the liquid-liquid boundary using light. Our interfacial design employs a dual-functional strategy to drive effective transformations of organic molecules. (1) The plasmonically active NPGB functions as a photothermal nanoheater, localizing heat at the liquid-liquid interface upon light irradiation. This targeted heating raises the interfacial temperature to activate the chemical reaction while maintaining the stability of the catalyst layer. (2) NPGB also doubles as a plasmonic catalyst, generating energetic hot carriers that accelerate reaction rates and direct reaction pathways. This multifunctional photothermal-plasmonic catalytic design diverges from traditional phase-boundary approaches, which typically depend on solid materials with singular catalytic properties or use emulsification to expand the interfacial contact.

Notably, incorporating nanoporous gold bowls (NPGB) at the liquid-liquid interface enables precise, localized heating of the interface to ~70°C using light. Our model biphasic reaction examines the reduction of organic-soluble 4-nitroaniline (4-NA) with aqueous $NaBH_4$ to produce paraphenylenediamine (PPD), a key industrial precursor for polymers, photographic developers, and dyes.[26-29] This photothermal-plasmonic system achieves a 36-fold increase in reactant consumption compared to the inherent reactivity of immiscible reactants, reaching up to 92% conversion to PPD within 90 minutes under optimized conditions. Systematic studies reveal that light-induced plasmonic and photothermal effects drive 90% of the overall reaction enhancement, while NPGB's intrinsic catalytic activity accounts for only 10%, highlighting the limitations of conventional phase-boundary catalysis. Mechanistic insights unravel distinct roles for heating and plasmonic effects: heating promotes borohydride anion release to generate hydride intermediates as active reductants, while plasmonic hot electrons further boost reaction efficiency and selectivity by enriching surface hydride species via the effective suppression of unwanted hydride hydrolysis to H_2 gas. Our work on photothermal-plasmonic design enables precise, light-driven control over reactions at the biphasic interface, thereby presenting a greener and more efficient approach for chemical manufacturing and environmental applications.

Results and Discussion

Our photothermal-plasmonic NPGB catalyst plays two essential roles in biphasic reactions by providing localized photothermal heating and serving as a plasmonic catalyst to enhance reaction kinetics and direct the reaction pathway (Figure 1A). We utilize nanoporous gold bowls (NPGBs) as phase-boundary catalysts due to their capacity to remotely convert light energy into both heat and hot carriers through the non-radiative decay of localized surface plasmon resonances. The heat generated is primarily confined within the interfacial region to thermally accelerate the phase-boundary catalysis (PBC) reaction, while the hot carriers interact with reagents to catalyze the transformation. We synthesize NPGBs via a two-step method that includes growing NPGBs on AgCl nanocubes as sacrificial templates with polyvinylpyrrolidone (PVP) as a capping agent, followed by chemical etching to remove the AgCl.[30] This synthesis yields NPGBs with semi-spherical, bowl-like structures (diameter: 346 ± 35 nm) and uniformly interdigitated gold ligaments (thickness: ~22 nm; Figure 1B, Figure S1). X-ray photoelectron spectroscopy (XPS) confirms the successful formation of NPGBs, displaying characteristic Au 4f peaks corresponding to metallic gold (Au^0; Figure S2). Additionally, diffuse reflectance spectroscopy (DRS) reveals broadband light absorption across the visible to near-infrared (450-1000 nm; Figure S3) spectrum, attributed to plasmonic resonances and extensive intra- and interparticle plasmonic coupling.

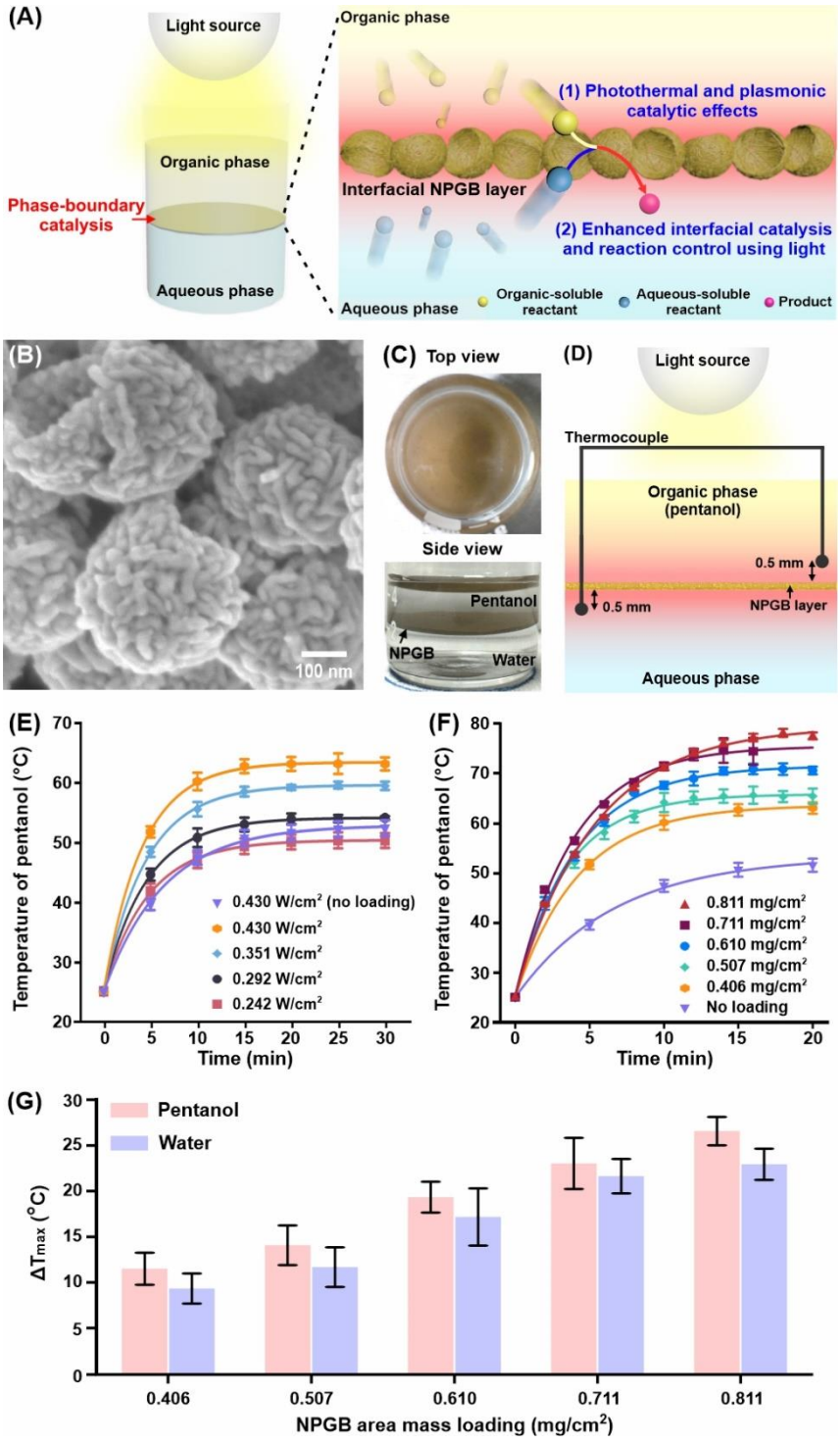

Figure 1. (A) Schematic illustrating the application of nanoporous gold bowls (NPGBs) as photothermal-plasmonic catalysts positioned at the immiscible liquid-liquid interface to facilitate efficient phase-boundary catalysis. (B) SEM image of as-synthesized NPGB. (C) Optical images

showing the top and side views of the NPGB layer (0.811 mg/cm^2) assembled at the water-pentanol phase boundary. (D) Schematic of the experimental setup used to simultaneously measure the temperature of both liquid phases near the interfacial NPGB layer. Time-dependent temperature profiles of the pentanol phase near the NPGB layer at different (E) light irradiances and (F) NPGB loadings. (G) Maximum temperature change achieved due to photothermal heating in both the pentanol and water phases at various NPGB loadings. The photothermal temperature is calculated as the temperature difference under light irradiation with and without the interfacial NPGB layer.

In phase-boundary catalysis, reactions primarily occur at the liquid-liquid interface, making it essential for the plasmonic NPGB catalyst to assemble uniformly along this boundary for optimal reactivity. The PVP on NPGBs' surfaces features both hydrophobic and hydrophilic moieties, allowing effective interaction with both organic and aqueous phases to promote uniform dispersion at the liquid-liquid boundary. Upon transferring NPGBs to the liquid-liquid interface, we observe that they rapidly spread and assemble across the interface, evenly covering the entire interfacial area (Figure 1C). This particle assembly remains stable, with NPGBs not dispersing into the bulk organic or aqueous phases. As the nanoparticle loading increases from 0.406 mg/cm^2 to 0.811 mg/cm^2 (Figure S4), the interfacial layer remains uniform but appears more opaque, indicating increased compactness with higher loading density. Forming this uniform and controllable interfacial nanoparticle layer is crucial for maximizing liquid-catalyst-liquid interactions and effectively modulating the photothermal heating process by the interfacial NPGB layer.

Next, we examine the NPGB's ability to absorb and convert light energy into hot carriers and heat upon plasmon decay, a critical factor for controlling and driving phase-boundary catalysis using light. Transmittance studies show that a thin NPGB layer with a mass loading of 0.811 mg/cm^2 has only 10% transmittance, indicating it effectively absorbs 90% of the light (Figure S5). This result aligns with our DRS findings, where broadband plasmon resonances enable efficient visible light absorption essential for photothermal and plasmonic catalysis. To assess NPGB's potential for generating energetic hot carriers, we measure photocurrent using a three-electrode photoelectrochemical setup with a 0.5 M Na_2SO_4 electrolyte under an applied potential of -1.3 V vs. Ag/AgCl. Upon light irradiation, we observe an immediate spike in photocurrent, indicating plasmon-induced hot carrier generation (Figure S6). The photocurrent stabilizes at around 200 μA/cm^2 during continuous irradiation and rapidly diminishes when the light is turned off, demonstrating NPGB's quick photoresponse in generating hot carriers. The plasmon-induced hot carrier generation process is highly reproducible, as shown by consistent photocurrent responses with <9% deviation over five successive on-off light cycles. These findings confirm that NPGBs effectively absorb light and generate hot carriers on-demand upon irradiation that can be harnessed to drive redox reactions in organic transformations.

NPGB also functions as an efficient plasmonic nanoheater at the liquid-liquid interface, controlling local interfacial temperature through photothermal conversion without disturbing the interfacial assembly. We use pentanol and water as the organic and aqueous phases, respectively, chosen for their immiscibility, high boiling points (138 °C for pentanol and 100 °C for water), and the relatively low toxicity and biodegradability of pentanol. Pentanol with lower density forms the upper organic phase above the aqueous layer. We measure the temperature near the interfacial NPGB layer upon light irradiation (Figure 1D) by positioning thermocouple probes

close to the particle layer (~0.5 mm) without direct contact to avoid disrupting the particle assembly. To optimize photothermal heating, we vary (i) light irradiance (with NPGB loading fixed at 0.406 mg/cm^2) and (ii) NPGB areal loading (with irradiance fixed at 0.430 W/cm^2). Temperature readings show that both liquid phases heat up quickly under white light irradiation (0.242 – 0.430 W/cm^2) and reach equilibrium within 10 minutes (Figure 1E, 1F; Figure S7). Higher light irradiance raises the interfacial temperature, with maximum equilibrium temperatures of ~63.0 °C in pentanol and 61.4 °C in water at 0.430 W/cm^2. This increase results from a greater photon supply at higher irradiance levels, though attempt to further increase irradiance is limited by technical constraints in positioning the LED light source closer to the NPGB layer. Moreover, increasing NPGB areal loading from 0.406 to 0.711 mg/cm^2 generally raises equilibrium temperatures in both phases. Further increasing NPGB loading to 0.811 mg/cm^2 yields similar temperatures (~78.0 °C in pentanol and 74.5 °C in water), indicating that subsequent increment in NPGB loading may hinder efficient heat transfer into the surrounding liquid media. We confirm that NPGB-mediated photothermal heating significantly contributes to local interfacial heating, adding up to ~25 °C (ΔT_{max}) at an NPGB loading of 0.811 mg/cm^2 and 0.430 W/cm^2 irradiance compared to baseline heating from the lamp alone (i.e., without the interfacial NPGB layer). NPGB-mediated photothermal heating is easily modulated (ΔT_{max}, 10 ^{o}C – 25 ^{o}C) by varying light irradiance, with the ΔT_{max} in pentanol slightly exceeding that in water due to pentanol's lower heat capacity ($C_{pentanol}$ = 2.4 J g^{-1} K^{-1}; C_{water} = 4.2 J g^{-1} K^{-1}; Figure 1G; Figure S8). The ability of NPGBs to deliver consistent, localized heating along the liquid-liquid boundary is essential for modulating reaction kinetics at the interface through precise temperature control. Hereon, we will use the optimized conditions of 0.430 W/cm^2 light

irradiance and NPGB areal loading of 0.811 mg/cm^2 for subsequent reaction studies as they provide the highest photothermal heating.

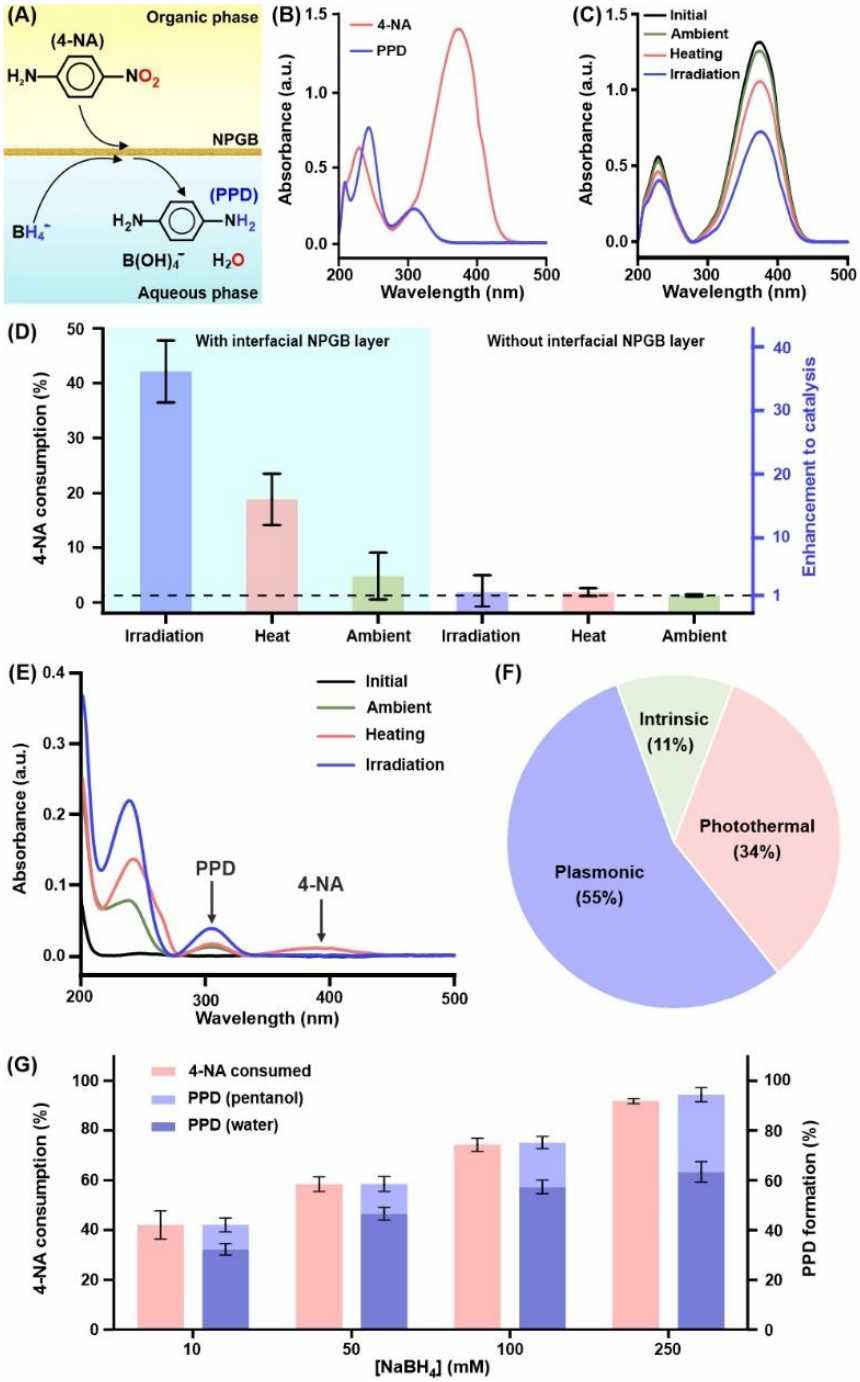

Figure 2. (A) Reaction scheme depicting the phase-boundary catalysis performed by the interfacial NPGB layer. The model reaction involves the reduction of 4-nitroaniline (4-NA) to

paraphenylenediamine (PPD). (B) UV-visible absorption spectra of 4-NA and PPD in pentanol. (C) UV-visible absorption spectra of the pentanol phase after 90 min in the presence of interfacial NPGB layer and 10 mM $NaBH_4$ as the reducing agent under different experimental conditions. (D) 4-NA reactant consumption in the pentanol phase after phase-boundary catalysis and their enhancement (compared to the ambient setup without NPGB) under different experimental conditions. (E) UV-visible absorption spectra of the aqueous phase after 90 min reaction under various experimental conditions. (F) Contribution of various factors (intrinsic catalytic property, photothermal effect, and plasmonic effect) to the overall catalytic performance of 4-NA reduction. (G) Comparison of 4-NA consumption and PPD present in both pentanol and aqueous phase at different $NaBH_4$ concentrations.

Having demonstrated NPGB's ability to generate hot carriers and deliver interfacial heating, we apply the photothermal-plasmonic catalyst at the liquid-liquid interface to drive multiphasic chemical reaction. Our phase-boundary catalysis involves the interfacial reduction of 4-nitroaniline (4-NA) by aqueous $NaBH_4$ to produce paraphenylenediamine (PPD), effectively coupling an organic-soluble reactant with a mild, environmentally benign aqueous reductant. This interfacial reaction design resolves typical reactant incompatibility and replaces hazardous reducing agents commonly used in organic phases (e.g., $LiAlH_4$, diisobutylaluminum hydride, H_2 gas) with a safer alternative. The experimental setup consists of three primary components: (i) a top pentanol layer containing 4-NA (1 mM), (ii) a photothermal-plasmonic catalyst layer uniformly dispersed at the liquid-liquid interface, and (iii) a bottom aqueous $NaBH_4$ solution acting as the reducing agent (Figure 2A). We monitor reaction progress using UV-visible absorption spectroscopy, tracking the decrease of the 4-NA peak at 375 nm in pentanol (Figure

2B, Figure S9) and the increase of the PPD peak at 306 nm in water or pentanol (Figure S10; Supplementary Text 1) based on calibration curves. This approach allows us to observe reactant consumption, product formation, and the migration of PPD into the aqueous phase as the reaction proceeds. With the interfacial NPGB layer and low $NaBH_4$ concentration (10 mM), we observe over 40% consumption of 4-NA under light irradiation for 90 min (Figure 2D). Product quantification confirms ~100% conversion of consumed 4-NA to PPD, which primarily accumulates in the aqueous phase due to increased hydrophilicity from amino group formation which allows the in situ extraction of the product from the organic reactant phase. In contrast, a control setup without the interfacial NPGB layer shows no loss of 4-NA from the pentanol phase (Figure S11), even under light irradiation. These comparisons confirm that phase-boundary catalysis effectively drives reactions between immiscible reactants, ruling out 4-NA loss from phase transfer into the aqueous solution (as 4-NA favors the organic pentanol phase) or light-induced degradation.

Notably, the enhanced interfacial reaction in our phase-boundary setup likely stems from three main factors: (i) the intrinsic catalytic activity of the Au catalyst, (ii) heat-mediated enhancement of reaction kinetics, and (iii) plasmonic catalysis using hot carriers to boost the reaction. To quantify each factor's contribution, we compare reaction performance across three conditions involving light irradiation only, bulk heating only, and ambient conditions (i.e., no heating or irradiation), both with and without an interfacial NPGB layer. We set bulk heating to 80 °C to approximate the maximum temperature (~78 °C) near the NPGB layer during localized photothermal heating. In the presence of the NPGB layer, light irradiation achieves the highest 4-NA consumption (42%; Figure 2C, 2D), which is double that observed with bulk heating alone (19%) and ~9-fold higher than ambient conditions (5%). Nearly all 4-NA molecules consumed

are converted into PPD (Figure 2E; Figure S12, S13, Supplementary 2), especially under light irradiation. Interestingly, bulk heating of the biphasic setup with the NPGB layer results in ~2% of 4-NA reactants migrating into the aqueous phase without undergoing chemical reaction, signifying that thermal heating alone lacks sufficient reactivity at the liquid phase boundary to effectively convert all reactants. In contrast, control setups without the NPGB layer show only minimal changes (~1-2%) in 4-NA levels across all three conditions (Figure S11), indicating that neither external heating nor irradiation alone enhances the inherent reactivity of the immiscible reactants.

More importantly, these comparisons clearly demonstrate that intrinsic catalytic, photothermal, and plasmonic effects are all crucial for enhancing the reaction at the liquid-liquid interface. For instance, when benchmarked against the catalyst-free setup, the NPGB layer under ambient conditions exhibits a ~5-fold increase in reaction activity, implying that the intrinsic catalytic activity of Au contributes ~11% to overall performance (Figure 2F; Supplementary Text 1). Bulk heating of the NPGB layer (i.e., combining both catalytic and heating effects) yields an ~18-fold enhancement, indicating that photothermal heating of the interface contributes ~34% to the overall reaction performance. Under light irradiation, the NPGB layer achieves a ~36-fold enhancement, highlighting that plasmonic effects account for ~55% of the total reaction performance as this setup integrates catalytic, photothermal, and plasmonic effects. The higher contribution of plasmonic effects over photothermal heating emphasizes that NPGB acts as more than a photothermal heater, whereby the plasmon-induced hot carriers also play a vital role in driving the biphasic reaction. This advantage is unattainable with traditional phase-boundary catalysis relying solely on bulk heating and materials with single catalytic function. It is also noteworthy that the combined plasmonic and photothermal effects contribute up to ~90% of the

overall reaction performance, underscoring that light and light-induced effects are crucial for enhancing biphasic reactions through our multifunctional photothermal-plasmonic catalyst.

To further enhance the interfacial reaction, we vary the $NaBH_4$ concentration from 10 mM to 250 mM and monitor the distribution of the reactant and product across the organic and aqueous phases. The higher $NaBH_4$ concentration drastically boosts 4-NA consumption, with the reductant at 250 mM achieving the highest 4-NA consumption at 92% (Figure 2G; Figure S14). Time-dependent UV-visible absorption spectra reveal an exponential decrease in 4-NA concentration, reaching equilibrium within 90 minutes under light irradiation which signifies reaction completion (Figure S15). This increase in 4-NA consumption is attributed to the higher availability of reactive hydride intermediates, which are crucial for the efficient reduction of the nitro group in 4-NA to the amine group in PPD. The PPD product is predominantly present in the aqueous phase (>70% of the total PPD generated) with a minor fraction in the organic phase (Figure 2G). More importantly, the combined PPD amount in both liquid phases matches the 4-NA consumed, providing clear evidence that nearly 100% of the 4-NA consumed is converted into the target PPD product. These results highlight the efficiency of the light-driven phase-boundary catalysis in rapidly converting 4-NA to PPD while preventing phase transfer of the reactant into the bulk aqueous phase, which could otherwise deactivate the reaction.

To gain deeper mechanistic insights into the reduction of 4-NA facilitated by the interfacial NPGB catalyst, we investigate the roles of hydride from $NaBH_4$ and plasmon-induced hot carriers (hot electrons or holes) in driving the reaction. First, we analyze the role of $NaBH_4$ by comparing its performance with alternative reducing agents such as sodium oxalate ($Na_2C_2O_4$) and sodium sulfite (Na_2SO_3). Control setups replacing $NaBH_4$ with either $Na_2C_2O_4$ or Na_2SO_3 (also at 250 mM) under light irradiation show only a 8% reduction in 4-NA in the pentanol layer

after 90 minutes, primarily due to the transfer of 4-NA into the aqueous phase (Figure 3A; Figure S16). These results provide two key insights: (1) The reaction is not solely driven by electron transfer from the reducing agents or plasmon-induced hot electrons generated by the NPGB catalyst, and (2) $NaBH_4$ serves as a crucial precursor to provide hydride as the active species driving the reduction reaction, rather than merely acting as a hole scavenger.

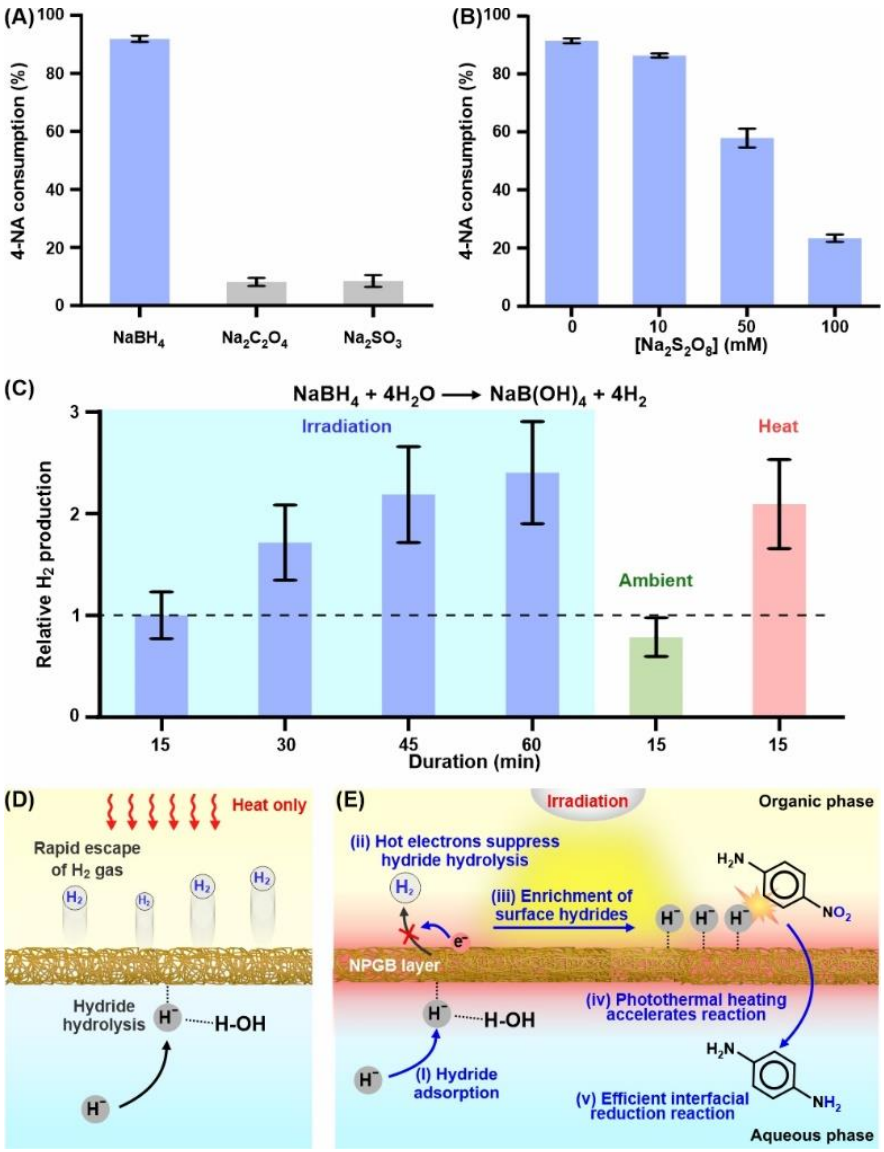

Figure 3. (A) 4-NA consumption during phase-boundary catalysis when $NaBH_4$ is replaced with other reducing agents. (B) 4-NA consumption in the presence of various $Na_2S_2O_8$ concentrations

as an electron scavenger alongside 250 mM $NaBH_4$. (C) Relative H_2 gas formation in the presence of the interfacial NPGB layer under various experimental conditions for 4-NA reduction (compared to the 15-minute irradiation). (D) Schematic illustrating the rapid hydride hydrolysis and formation of H_2 gas as a side reaction when subjected to heat only. (E) Proposed mechanism for the enhanced 4-NA reduction by interfacial NPGB photothermal-plasmonic catalysts under light irradiation.

Notably, plasmon-induced hot electrons also play an indispensable role in the 4-NA reduction reaction. This is evident from the lack of 4-NA reduction when using $NaBH_4$ in the absence of the interfacial NPGB layer. Furthermore, control experiments with increasing concentrations of an electron scavenger (e.g., sodium persulfate; $Na_2S_2O_8$; 10 – 100 mM) in the aqueous phase alongside 250 mM $NaBH_4$ reveal a drastic suppression of the reaction (Figure 3B; Figure S17). At 100 mM $Na_2S_2O_8$, 4-NA consumption drops to <16% with no apparent formation of PPD (Figure S18). The observed decrease in 4-NA consumption correlates directly with the removal of plasmon-induced hot electrons by the electron scavenger, underscoring their critical role in driving the interfacial reaction. These findings highlight that the NPGB catalyst's function extends beyond serving as an electron relay or providing active sites, whereby its ability to generate and harness plasmon-induced hot electrons is crucial for enabling efficient reduction reactions at the liquid-liquid interface.

Thus far, our results confirm that both hydride and plasmon-induced hot electrons are critical for driving the reduction of 4-NA. Since hydride is negatively charged and cannot undergo further reduction, hot electrons likely enhance its availability for the reduction reaction

by suppressing its side reactions. This role is particularly crucial because hydride is prone to hydrolysis by water, producing H_2 gas as a side product (Figure 3C), as previously reported in the literature. To investigate the role of plasmon-induced hot electrons in suppressing hydride hydrolysis, we quantify H_2 gas produced during the reaction using gas chromatography (GC) at 15-minute intervals over 60 minutes. We compare three setups containing an interfacial NPGB layer: (i) under light irradiation (with plasmonic and photothermal effects), (ii) under external heating only (thermal effect), and (iii) at ambient conditions (representing intrinsic $NaBH_4$ degradation into H_2 gas). Under light irradiation, H_2 production increases gradually by ~2.4-fold from the initial value at 15 min by the end of 60 minutes, confirming that hydride hydrolysis indeed occurs as a side reaction (Figures 3C, Figure S19). In contrast, external heating at 80 °C in the dark generates nearly 3-fold more H_2 gas within 15 minutes compared to the ambient setup (Figures S20, S21), indicating that heating accelerates both the reduction of 4-NA and hydride-to-H_2 conversion (Figure 3D). More importantly, comparing setups under light irradiation and external heating at the 15-minute mark reveals significantly lower H_2 production under irradiation, despite the presence of both plasmonic and photothermal effects. This finding demonstrates that plasmon-induced hot electrons effectively suppress unwanted hydride hydrolysis and H_2 formation. This phenomenon likely occurs as hot electrons transfer to the H_2 side product, regenerating hydride at the NPGB surface under light irradiation. This regeneration process consequently increases the abundance of the surface gold-hydride intermediate, a key factor in promoting the interfacial 4-NA reduction reaction.

Our comprehensive investigations collectively elucidate the mechanism by which the photothermal-plasmonic NPGB catalyst enhances the 4-NA reduction process at the liquid-liquid boundary. This reaction enhancement arises from the plasmonic resonances that generate both

localized heating and hot electrons directly at the point-of-reaction (Figure 3E). The reaction employs $NaBH_4$ as the hydride source, which adsorbs onto the catalyst surface to form a gold-hydride intermediate as the active reductant for 4-NA reduction. Upon light irradiation, photothermal heating also increases the local temperature at the liquid interface which accelerates the reduction of 4-NA by hydride ions, as demonstrated in both externally heated and irradiated setups. However, elevated temperatures also promote the protonation of gold-hydride intermediate, leading to H_2 gas formation and its subsequent escape from the system. This side reaction reduces the availability of surface hydrides and limits the efficiency of the interfacial reaction. Notably, plasmon-induced hot electrons generated by the NPGB catalyst under light irradiation effectively address this limitation. These hot electrons suppress the loss of active surface hydrides by reducing H_2 gas back into hydride ions. Such regeneration of surface hydrides enriches the catalyst surface, drastically boosting its ability to drive efficient interfacial reduction reactions. The synergistic effects of surface hydride enrichment and localized heating under light irradiation result in an >8-fold improvement in 4-NA reduction compared to the ambient setup, even with the same interfacial NPGB layer. Our findings clearly demonstrate that plasmonic hot electrons not only suppress side reactions but also synergistically enhance the primary reduction process. This dual functionality firmly establishes the photothermal-plasmonic NPGB catalyst as a highly effective tool for driving and manipulating phase-boundary catalysis with light.

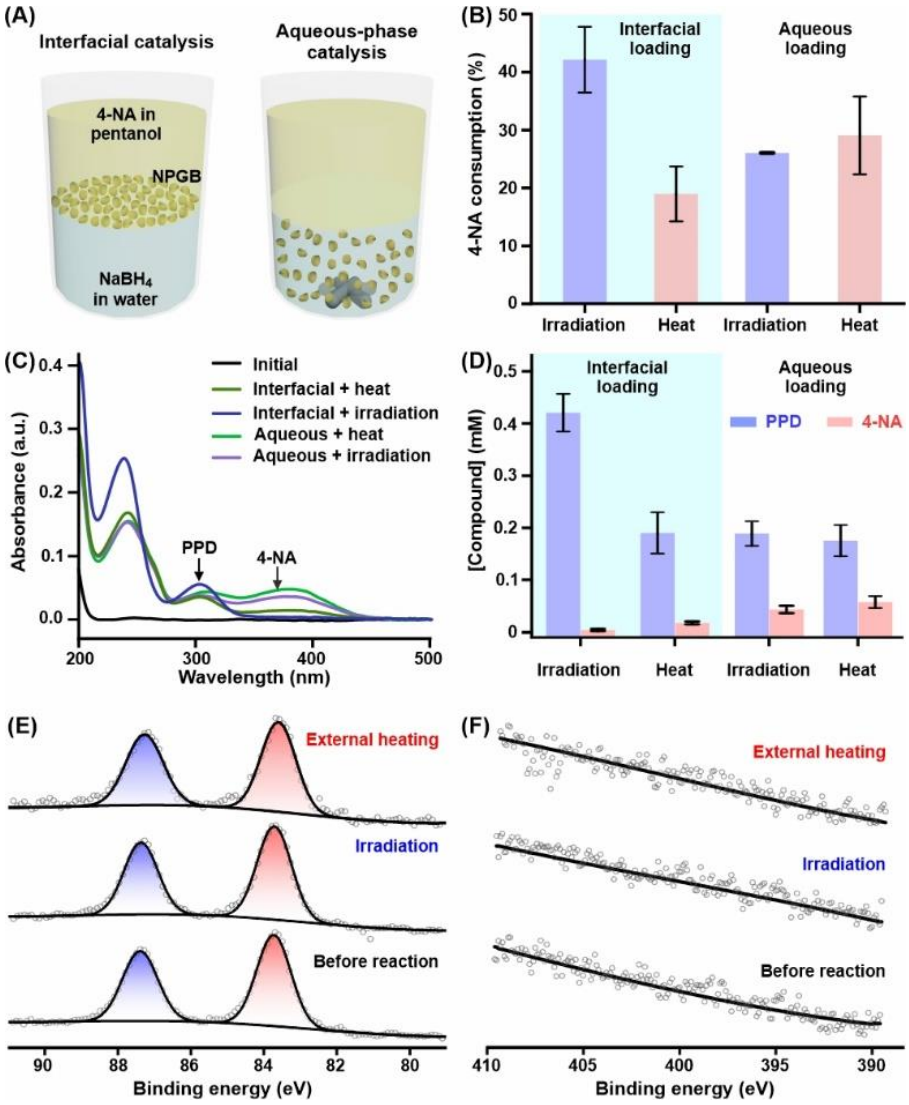

Figure 4. (A) Schematic illustrating the comparison between interfacial NPGB layer and NPGB loaded only in the aqueous phase. (B) Consumption of 4-NA reactant in the pentanol phase for the two experimental setups shown in (A). (C) UV-visible absorption spectra showing the formation of PPD and the transfer of 4-NA in the aqueous phase. (D) Corresponding concentrations of PPD product and 4-NA reactant present in the aqueous phase. High-resolution XPS spectra of (E) Au 4f and (F) N 1s before and after 4-NA reduction under either heat or light irradiation.

Finally, we emphasize the critical role of phase-boundary catalysis by comparing it with a control setup where the same NPGB catalyst is suspended in the bulk aqueous phase rather than positioned at the liquid-liquid interface (Figure 4A). NPGB placement in the organic phase is not viable for direct comparison, as the catalyst naturally settles at the interface due to gravity. In the control setups, gentle stirring at 100 rpm ensures uniform suspension of NPGB in the aqueous phase and the $NaBH_4$ concentration is standardized at 10 mM across all experiments. Under light irradiation, the phase-boundary catalytic setup achieves ~2-fold higher 4-NA consumption compared to the control setups where NPGB is suspended in the aqueous phase, under either light irradiation or external heating (both show ~26% 4-NA consumption; Figures 4B, Figure S22). Additionally, external heating of the phase-boundary catalytic setup (without light irradiation) and both aqueous-phase control setups reveal unreacted 4-NA in the aqueous phase (Figure 4C, 4D), indicating phase-transfer losses of 4-NA (up to 25% of total 4-NA consumption) from the organic phase. We also note similar amounts of PPD are formed in the aqueous phase across all three control setups (Figure 4D). The unreacted 4-NA in the aqueous phase highlights the inefficiency of biphasic systems with NPGB suspended only in the aqueous phase. Lower solubility of 4-NA in water and additional diffusion barriers hinder phase-transfer processes, reducing the effective 4-NA concentration in the aqueous phase and thereby limiting the reaction rate. More importantly, similar PPD formation in aqueous-phase control setups under both external heating and light irradiation underscores the absence of plasmon-induced hot electron effects for hydride regeneration. This observation likely arises from the abundance of water molecules surrounding the entire catalyst which rapidly hydrolyzes active surface hydrides and consequently inhibits the 4-NA reduction reaction. These comparisons jointly underscore the importance of strategically positioning the photothermal-plasmonic catalyst at the liquid-liquid

interface to enable efficient interfacial reaction, notably by mitigating solubility challenges and directing selective reaction pathways using light. Our multifunctional NPGB catalysts also exhibit excellent physical and chemical robustness. SEM images show no structural changes to NPGB or its ligaments after the reaction (Figure S23), and XPS spectra confirm no shifts in Au 4f binding energies (Figure 4E). Additionally, no nitrogen signals are detected post-reaction, confirming the absence of catalyst poisoning by reactants or nitrogenous intermediates (Figure 4F).

Conclusion

In conclusion, we have successfully implemented multifunctional NPGB catalysts at liquid-liquid interfaces to boost phase-boundary catalysis through light-driven photothermal heating and plasmonic hot carrier generation. The NPGB catalyst serves to localize heat and generate hot electrons directly at the reaction interface, enabling precise modulation of interfacial temperature and efficient biphasic chemical transformations. Our photothermal-plasmonic approach achieves a ~36-fold improvement in the reduction of 4-nitroaniline (4-NA) to para-phenylenediamine (PPD) compared to ambient conditions, with plasmonic (55%) and photothermal (34%) effects as major contributors to the enhanced catalysis. This strategy effectively addresses the limitations of conventional phase-boundary catalysis reliant on singular catalytic properties. The strategic positioning of the NPGB catalyst at the liquid-liquid boundary also achieves a ~2-fold higher 4-NA consumption than bulk-phase suspensions, overcoming solubility challenges and enabling efficient coupling of reactants with polarity disparity. Mechanistic studies reveal that the enhanced catalysis arises from synergistic effects between surface hydride enrichment and localized heating under light irradiation. This dual functionality

firmly establishes the photothermal-plasmonic NPGB catalyst as a powerful tool for achieving and directing interfacial catalysis. Our work offers valuable insights into unlocking novel and efficient chemistries, thereby advancing molecular transformations under mild conditions previously deemed inaccessible. Achieving these benefits paves the way for more sustainable processes across diverse chemical, environmental, and energy applications.

Methods

Chemicals

Polyvinylpyrrolidone (PVP; MW = 1,300,000), hydroquinone (≥ 99%), ethylene glycol (anhydrous, 99.8%), silver nitrate ($AgNO_3$; ≥ 99%), gold(III) chloride trihydrate (≥ 99.9%), ammonium hydroxide (28.0 - 30.0%), pentanol (≥ 99%), 4-nitroaniline (≥ 99%), paraphenylenediamine (98%), sodium borohydride (99%), sodium oxolate (99.5%), sodium sulfite (≥ 98%), and sodium persulfate (≥ 98%) were purchased from Sigma-Aldrich. Ethanol (≥ 99.8%, absolute) was obtained from Thermo Fisher Scientific. All chemicals were used without further purification. Milli-Q water (> 18.0 MΩ. cm) was purified with a Sartorius Arium 611 ® UV ultrapure water system.

Synthesis of silver chloride (AgCl) nanocubes

0.4 g of PVP was first dissolved in 50 mL of cold ethylene glycol. To this solution, 0.4 g of $AgNO_3$ was added and allowed to fully dissolve. Subsequently, 1 mL of 37% hydrochloric acid (HCl) was added dropwise into the mixture, followed by stirring for 1 min. The resulting solution was then heated to 150 °C with stirring at 500 rpm for 20 min. After the mixture was

cooled to room temperature, the resulting suspension was washed thoroughly with acetone via repeated centrifugation steps.

Synthesis of nanoporous gold bowls (NPGBs)

0.554 mL of AgCl nanocube solution (6 mg mL^{-1}), 0.640 mL of hydroquinone solution (28 mM), and 0.400 mL of $HAuCl_4$ solution (40.372 mM) were sequentially added to 4.5 mL of PVP solution (63 mM) under stirring at room temperature. The mixture was stirred for 1 min, during which the colour of the reaction solution changed to dark grey. The resultant particles were collected by centrifugation and washed thoroughly with water. To remove the AgCl template, 2 mL of ammonia solution was added to the particle suspension. The colloidal solution was centrifuged again and washed with copious amounts of water. Finally, the particles were dispersed in 5 mL of ethanol for further use.

Preparation of the NPGB for photocurrent measurements

The NPGB nanoparticles were drop-casted onto a glassy carbon working electrode (diameter = 1 cm) and dried in an oven. The photoelectrochemical measurements were performed in a setup consisting of an aqueous Na_2SO_4 electrolyte solution (0.5 M), the glassy carbon working electrode, a platinum (Pt) wire counter electrode, and an Ag/AgCl (3 M) reference electrode. For photocurrent measurements, a potential of -1.3V (vs. Ag/AgCl) was applied to the system under 100W white light LED irradiation (400 – 750 nm). Data acquisition was carried out at 0.01 s intervals.

Photothermal heating measurement of NPGBs at the liquid-liquid interface

In this experiment, 2 mL of water was first added to a 10 mL glass beaker. Next, 0.1 mL of NPGB suspension in pentanol was placed on the surface of the aqueous layer to give an areal loading of 0.406 – 0.811 mg/cm². Following this, 1.9 mL of pentanol was added on top of the NPGB layer. Thermocouple thermometer probes were placed 0.5 mm above and below the NPGB layer at the pentanol-water interface. The distance between the NPGB layer and a 100W white LED light was adjusted between 4 and 7 cm by varying the height of the experimental setup. After the LED was switched on, the temperatures of both pentanol and aqueous phases was recorded at 2-minute intervals to observe the photothermal effect.

Quantification of 4-nitroaniline and paraphenylenediamine using UV-visible absorption spectroscopy

A calibration curve correlating extinction intensity to the concentration of 4-nitroaniline or paraphenylenediamine was first established to quantify these species during the catalytic reduction of 4-nitroaniline. Stock solutions of both 4-nitroaniline and paraphenylenediamine were prepared by dissolving the compounds in either pentanol or water. These solutions were serially diluted to obtain concentrations ranging from 0.2 mM to 1 mM. The absorption spectra were recorded using UV-visible absorption spectroscopy, and the characteristic peaks of each species were identified for quantification. 4-nitroaniline exhibited absorption peaks at 374 nm when dissolved in pentanol and 379 nm in water, while paraphenylenediamine showed absorption peaks at 309 nm in pentanol and 304 nm in water. These characteristic peaks were used to monitor the reactant and product concentrations in the catalytic reactions.

Phase-boundary catalysis using interfacial NPGB layer for the biphasic reduction of 4-nitroaniline

In this experiment, NPGBs were first dried and subsequently re-dispersed in a pentanol solution containing 1 mM of 4-nitroaniline. A 0.1 mL aliquot of this suspension was layered onto the surface of 2 mL of aqueous $NaBH_4$ solution, which served as the reducing agent. An additional 1.9 mL of the pentanol solution containing 4-nitroaniline was added on top of the NPGB layer, forming the interfacial catalytic layer. The reaction setup was then exposed to 100 W LED white for 90 min to initiate the reduction of 4-nitroaniline. After the reaction, both the organic (i.e., pentanol) and aqueous phases were collected and analyzed using UV-visible absorption spectroscopy to determine the concentrations of 4-nitroaniline and paraphenylenediamine. Each experiment was conducted in triplicate to ensure the accuracy and reproducibility of the results.

Quantification of hydrogen (H_2) produced during the 4-nitroaniline reduction reaction

The reduction of 4-nitroaniline was conducted using the previously described method but with the reaction performed in a 12 mL transparent quartz tube sealed with a septum. The reaction vessel was tilted at a 45° angle and irradiated from the top with a 100 W white LED light to initiate the photocatalysis. After the reaction, the produced gas was sampled by withdrawing 1.0 mL of the headspace gas from the reactor and injecting it into a gas chromatograph (SRI Multiple Gas Analyzer #5) equipped with a thermal conductivity detector (GC-TCD). The GC peak areas and H_2 concentrations were adjusted by subtracting background interferences from the instrument. All experiments were conducted in triplicate to ensure the reliability and reproducibility of the H_2 quantification results.

Characterization

Scanning electron microscopy (SEM) characterizations were performed using a JEOL-JSM-7600F microscope. UV-visible spectroscopic measurements were conducted using an AvaSpec-ULS2048CL-EVO-UA-50 equipped with a deuterium-halogen light source (AvaLight-DH-S). Diffuse reflectance measurements were performed with the same spectrometer and an integrating sphere containing a halogen light source (AvaSphere-50-LS-HAL-12V). X-ray photoelectron spectroscopy (XPS) characterizations were carried out using a Phoibos 100 spectrometer with a monochromatic Mg X-ray radiation source. All XPS spectra were calibrated using the high-resolution C 1s peak at 284.5 eV as a reference. Photocurrent measurements were conducted with a Metrohm PGSTAT204 potentiostat. A thermocouple thermometer (UNI-T UT3200) was used to measure the temperature of the reaction setup during light irradiation. Gas chromatography (GC) measurements were conducted using a SRI Multiple Gas Analyzer #5 equipped with a thermal conductivity detector (GC-TCD).

Supporting Information

The following files are available free of charge.

The characterization of photothermal plasmonic NPGB catalysts, investigation of the effect of photothermal heating effect of NPGB on both the organic and aqueous solution, quantification of 4-nitroaniline and paraphenylenediamine using UV-visible absorption spectroscopy, phase-boundary catalysis for the biphasic 4-nitroaniline reduction reaction using photothermal hydrogen plasmonic NPGB catalysts, gas suppression by the photothermal plasmonic NPGB catalysts and characterization (PDF)

REFERENCES

1. Wiebe, A.; Gieshoff, T.; Möhle, S.; Rodrigo, E.; Zirbes, M.; Waldvogel, S. R., Electrifying Organic Synthesis. *Angew. Chem. Int. Ed.* **2018,** *57* (20), 5594-5619.

2. Dedovets, D.; Li, Q.; Leclercq, L.; Nardello-Rataj, V.; Leng, J.; Zhao, S.; Pera-Titus, M., Multiphase Microreactors Based on Liquid–Liquid and Gas–Liquid Dispersions Stabilized by Colloidal Catalytic Particles. *Angew. Chem. Int. Ed.* **2022,** *61* (4), e202107537.

3. Zhang, Y.; Ye, Z.; Li, C.; Chen, Q.; Aljuhani, W.; Huang, Y.; Xu, X.; Wu, C.; Bell, S. E. J.; Xu, Y., General approach to surface-accessible plasmonic Pickering emulsions for SERS sensing and interfacial catalysis. *Nat. Commun.* **2023,** *14* (1), 1392.

4. Duan, Y.; Luo, S., Phase-Transfer Catalysis for Electrochemical Chlorination and Nitration of Arenes. *Angew. Chem. Int. Ed.* **2024,** *63* (17), e202319206.

5. Shao, C.; Yu, X.; Ji, Y.; Xu, J.; Yan, Y.; Hu, Y.; Li, Y.; Huang, W.; Li, Y., Perfluoroalkyl-modified covalent organic frameworks for continuous photocatalytic hydrogen peroxide synthesis and extraction in a biphasic fluid system. *Nat. Commun.* **2024,** *15* (1), 8023.

6. Nur, H.; Ikeda, S.; Ohtani, B., Phase-boundary catalysis: a new approach in alkene epoxidation with hydrogen peroxide by zeolite loaded with alkylsilane-covered titanium oxide. *Chem. Commun.* **2000,** (22), 2235-2236.

7. Ikeda, S.; Nur, H.; Sawadaishi, T.; Ijiro, K.; Shimomura, M.; Ohtani, B., Direct Observation of Bimodal Amphiphilic Surface Structures of Zeolite Particles for a Novel Liquid−Liquid Phase Boundary Catalysis. *Langmuir* **2001,** *17* (26), 7976-7979.

8. Choi, K.-M.; Ikeda, S.; Ishino, S.; Ikeue, K.; Matsumura, M.; Ohtani, B., Oxidation of hydrophobic alcohols using aqueous hydrogen peroxide over amphiphilic silica particles loaded

with titanium(IV) oxide as a liquid–liquid phase-boundary catalyst. *Appl. Catal. A Gen.* **2005,** *278* (2), 269-274.

9. Zapata, P. A.; Faria, J.; Ruiz, M. P.; Jentoft, R. E.; Resasco, D. E., Hydrophobic Zeolites for Biofuel Upgrading Reactions at the Liquid–Liquid Interface in Water/Oil Emulsions. *J. Am. Chem. Soc.* **2012,** *134* (20), 8570-8578.

10. Zhang, P.; Chen, X.; Leng, Y.; Dong, Y.; Jiang, P.; Fan, M., Biodiesel production from palm oil and methanol via zeolite derived catalyst as a phase boundary catalyst: An optimization study by using response surface methodology. *Fuel* **2020,** *272*, 117680.

11. Pupo, G.; Ibba, F.; Ascough, D. M. H.; Vicini, A. C.; Ricci, P.; Christensen, K. E.; Pfeifer, L.; Morphy, J. R.; Brown, J. M.; Paton, R. S.; Gouverneur, V., Asymmetric nucleophilic fluorination under hydrogen bonding phase-transfer catalysis. *Science* **2018,** *360* (6389), 638-642.

12. Egami, H.; Rouno, T.; Niwa, T.; Masuda, K.; Yamashita, K.; Hamashima, Y., Asymmetric Dearomative Fluorination of 2-Naphthols with a Dicarboxylate Phase-Transfer Catalyst. *Angew. Chem. Int. Ed.* **2020,** *59* (33), 14101-14105.

13. Roagna, G.; Ascough, D. M. H.; Ibba, F.; Vicini, A. C.; Fontana, A.; Christensen, K. E.; Peschiulli, A.; Oehlrich, D.; Misale, A.; Trabanco, A. A.; Paton, R. S.; Pupo, G.; Gouverneur, V., Hydrogen Bonding Phase-Transfer Catalysis with Ionic Reactants: Enantioselective Synthesis of γ-Fluoroamines. *J. Am. Chem. Soc.* **2020,** *142* (33), 14045-14051.

14. Vicini, A. C.; Pupo, G.; Ibba, F.; Gouverneur, V., Multigram synthesis of N-alkyl bis-ureas for asymmetric hydrogen bonding phase-transfer catalysis. *Nat. Protoc.* **2021,** *16* (12), 5559-5591.

15. Tan, X.; Wang, Q.; Sun, J., Electricity-driven asymmetric bromocyclization enabled by chiral phosphate anion phase-transfer catalysis. *Nat. Commun.* **2023,** *14* (1), 357.

16. Vaida, V., Prebiotic phosphorylation enabled by microdroplets. **2017,** *114* (47), 12359-12361.

17. Schrimpf, M.; Graefe, P. A.; Holl, A.; Vorholt, A. J.; Leitner, W., Effect of Liquid–Liquid Interfacial Area on Biphasic Catalysis Exemplified by Hydroformylation. *ACS Catal.* **2022,** *12* (13), 7850-7861.

18. Nur, H.; Ikeda, S.; Ohtani, B., Phase-Boundary Catalysis of Alkene Epoxidation with Aqueous Hydrogen Peroxide Using Amphiphilic Zeolite Particles Loaded with Titanium Oxide. *J. Catal.* **2001,** *204* (2), 402-408.

19. Yuan, L. S.; Razali, R.; Efendi, J.; Buang, N. A.; Nur, H., Temperature-controlled selectivity in oxidation of 1-octene by using aqueous hydrogen peroxide in phase-boundary catalytic system. *Appl. Catal. A Gen.* **2013,** *460-461*, 21-25.

20. Hachiya, H.; Kon, Y.; Ono, Y.; Takumi, K.; Sasagawa, N.; Ezaki, Y.; Sato, K., Unique Salt Effect on the High Yield Synthesis of Acid-Labile Terpene Oxides Using Hydrogen Peroxide under Acidic Aqueous Conditions. *Synlett* **2011,** *2011* (19), 2819-2822.

21. Sen, S.; Pradhan, N. C.; Patwardhan, A. V., Kinetics of reaction of benzyl chloride with H2S-rich aqueous monoethanolamine: selective synthesis of dibenzyl sulfide under liquid–liquid phase-transfer catalysis. *Asia-Pac. J. Chem. Eng.* **2011,** *6* (2), 257-265.

22. Demirci, U. B.; Akdim, O.; Andrieux, J.; Hannauer, J.; Chamoun, R.; Miele, P., Sodium Borohydride Hydrolysis as Hydrogen Generator: Issues, State of the Art and Applicability Upstream from a Fuel Cell. *Fuel Cells* **2010,** *10* (3), 335-350.

23. Chen, W.; Ouyang, L. Z.; Liu, J. W.; Yao, X. D.; Wang, H.; Liu, Z. W.; Zhu, M., Hydrolysis and regeneration of sodium borohydride (NaBH4) – A combination of hydrogen production and storage. *J. Power Sources* **2017,** *359*, 400-407.

24. Ouyang, L.; Jiang, J.; Chen, K.; Zhu, M.; Liu, Z., Hydrogen Production via Hydrolysis and Alcoholysis of Light Metal-Based Materials: A Review. *Nanomicro Lett.* **2021,** *13* (1), 134.

25. Al-Msrhad, T. M. H.; Devrim, Y.; Uzundurukan, A.; Budak, Y., Investigation of hydrogen production from sodium borohydride by carbon nano tube-graphene supported PdRu bimetallic catalyst for PEM fuel cell application. *Int. J. Energy Res.* **2022,** *46* (4), 4156-4173.

26. Smiley, R. A., Phenylene- and Toluenediamines. In *Ullmann's Encyclopedia of Industrial Chemistry*, 2000.

27. Lunar, L.; Rubio, S.; Pérez-Bendito, D.; Jiménez, C., Identification of the main by-products of the developing agent N-hydroxyethyl-N-ethyl-3-methyl-p-phenylenediamine in photographic effluents by liquid chromatography/mass spectrometry. *Rapid Commun. Mass Spectrom.* **2002,** *16* (17), 1622-30.

28. Al-Suwaidi, A.; Ahmed, H., Determination of para-phenylenediamine (PPD) in henna in the United Arab Emirates. *Int J Environ Res Public Health* **2010,** *7* (4), 1681-93.

29. Stejskal, J., Polymers of phenylenediamines. *Prog. Polym. Sci.* **2015,** *41*, 1-31.

30. Pedireddy, S.; Lee, H. K.; Tjiu, W. W.; Phang, I. Y.; Tan, H. R.; Chua, S. Q.; Troadec, C.; Ling, X. Y., One-step synthesis of zero-dimensional hollow nanoporous gold nanoparticles with enhanced methanol electrooxidation performance. *Nat. Commun.* **2014,** *5* (1), 4947.

AUTHOR INFORMATION

Corresponding Author

Hiang Kwee Lee − Division of Chemistry and Biological Chemistry, School of Chemistry, Chemical Engineering and Biotechnology, Nanyang Technological University, 21 Nanyang Link, Singapore 637371 (Singapore). Email: hiangkwee@ntu.edu.sg

Author

Zhi Zhong Ang − Division of Chemistry and Biological Chemistry, School of Chemistry, Chemical Engineering and Biotechnology, Nanyang Technological University, 21 Nanyang Link, Singapore 637371 (Singapore).

Veronica Pereira− Division of Chemistry and Biological Chemistry, School of Chemistry, Chemical Engineering and Biotechnology, Nanyang Technological University, 21 Nanyang Link, Singapore 637371 (Singapore).

Li Shiuan Ng − Division of Chemistry and Biological Chemistry, School of Chemistry, Chemical Engineering and Biotechnology, Nanyang Technological University, 21 Nanyang Link, Singapore 637371 (Singapore).

Carice Chong − Division of Chemistry and Biological Chemistry, School of Chemistry, Chemical Engineering and Biotechnology, Nanyang Technological University, 21 Nanyang Link, Singapore 637371 (Singapore).

Haitao Li − School of Chemistry and Chemical Engineering, Yangzhou University, Yangzhou, 25002 (P. R. China).

Hongjian Yu − School of Chemistry and Chemical Engineering, Yangzhou University, Yangzhou, 25002 (P. R. China).

Author Contributions

The manuscript was written through the contributions of all authors. All authors have given approval to the final version of the manuscript.

ACKNOWLEDGMENT

H.K.L. thanks the funding supports from the Singapore Ministry of Education (AcRF Tier1 RS13/20 and RG4/21), the A*STAR Singapore (AME YIRG A2084c0158 and MTC IRG M23M6c0098), National University of Singapore Center of Hydrogen Innovation (CHI-P2022-05), and the Nanyang Technological University start-up grants. The research was conducted as a part of NICES (NTU-IMRE Chemistry Lab for EcoSustainability; REQ0275931), a joint research initiative between the Nanyang Technological University (NTU) and the Institute of Materials Research and Engineering (IMRE) from Agency for Science, Technology and Research (A*STAR).